Temperature dependence of small harmonically trapped atom systems with Bose, Fermi, and Boltzmann statistics

Yangqian Yan and D. Blume

Department of Physics and Astronomy, Washington State University, Pullman, Washington 99164-2814, USA

While the zero-temperature properties of harmonically trapped cold few-atom systems have been discussed fairly extensively over the past decade, much less is known about the finite-temperature properties. Working in the canonical ensemble, we characterize small harmonically trapped atomic systems as a function of the temperature using analytical and numerical techniques. We present results for the energetics, structural properties, condensate fraction, superfluid fraction, and superfluid density. Our calculations for the two-body system underline that the condensate and superfluid fractions are distinctly different quantities. Our work demonstrates that the path-integral Monte Carlo method yields reliable results for bosonic and fermionic systems over a wide temperature range, including the regime where the de Broglie wavelength is large, i.e., where the statistics plays an important role. The regime where the Fermi sign problem leads to reasonably large signal-to-noise ratios is mapped out for selected parameter combinations. Our calculations for bosons focus on the unitary regime, where the physics is expected to be governed by the three-body parameter. If the three-body parameter is large compared to the inverse of the harmonic oscillator length, we find that the bosons form a droplet at low temperature and behave approximately like a noninteracting Bose and eventually Boltzmann gas at high temperature. The change of the behavior occurs over a fairly narrow temperature range. A simple model that reproduces the key aspects of the phase-transition-like feature, which can potentially be observed in cold atom Bose gas experiments, is presented.

PACS number(s): 03.75.−b

I. INTRODUCTION

Ultracold atomic gases provide a flexible platform for studying a myriad of phenomena that are driven by quantum mechanics [1–6]. Generally speaking, quantum statistical effects dominate when the de Broglie wavelength is comparable to or larger than the average interparticle spacing. When the de Broglie wavelength is small, the particle statistics plays a negligible role and the system dynamics is governed by Boltzmann statistics. Since the de Broglie wavelength scales as $1/\sqrt{T}$ [2,3], where T is the temperature, changing the temperature allows one to turn the particle statistics "on" and "off." Atomic gases, which can be cooled to below the quantum degeneracy temperature, thus provide an ideal platform for investigating the importance of particle statistics.

For macroscopic samples, a prominent example for a thermal phase transition is the transition from the normal to the superfluid phase as observed in bosonic liquid ^{4}He and fermionic liquid ^{3}He [7]. Bose-Einstein condensation, the macroscopic occupation of a single-particle state, is another important example. While Bose-Einstein condensation occurs for ultracold bosonic atomic gases [1], it does not occur, at least not directly, for ultracold fermionic atomic gases [5,8]. Condensation for fermions occurs only when two fermions form composite bosons (diatomic molecules or Cooper pairs) [5,8–10]. If the number of particles is finite (as opposed to infinite), phase transitions get smeared out and the usual concept, which considers statistical properties in the thermodynamic limit, has to be revised [11,12].

The main objective of this paper is to study the temperature dependence of small harmonically trapped atomic Bose and Fermi systems. To describe these systems, we adopt the canonical ensemble, i.e., we assume that the system under study is in thermal contact with a heat bath or thermostat, which has a large number of particles and a well-defined temperature

T [13]. We monitor various system properties as a function of the temperature, the number of particles, the particle statistics, and the interaction strength. Particular emphasis is placed on the strongly interacting unitary regime, where the s-wave scattering length diverges. At zero temperature, it is well established that the particle statistics has a paramount effect on the system properties. Two-component Fermi gases with infinitely large interspecies scattering length are fully described by the s-wave scattering length alone [4,5,14–16], while the properties of Bose gases additionally depend on a three-body parameter [17,18]. These fundamental differences, which are due to the particle statistics, continue to play an important role at low temperature but die out at sufficiently high temperature. An interesting question, which we attempt to answer in this paper, is thus what happens at intermediate temperatures. As expected, we find that the low- and intermediate-temperature behavior of Bose and Fermi gases is vastly different. For certain parameter combinations, we find a thermal phase-transition-like feature for Bose systems that is governed by the three-body Efimov parameter. Specifically, we find a transition from a dropletlike state to a gaslike state. No such transition exists for two-component Fermi gases.

The remainder of this paper is organized as follows. Section II introduces the system Hamiltonian and reviews the connections between the free-space Efimov spectrum and the zero-temperature spectrum of the harmonically trapped three-boson system. Moreover, the path-integral Monte Carlo (PIMC) approach is introduced and some numerical details are discussed. Section III presents finite-temperature characteristics of the trapped two-atom system. Emphasis is placed on the condensate and superfluid fractions. The radial superfluid density is calculated and analyzed. Section IV discusses our finite-temperature results for systems with three and more particles. Section IV A focuses on systems consisting of N identical bosons, while Sec. IV B considers a trapped gas with

Bose, Fermi, or Boltzmann statistics with an impurity. Lastly, Sec. V concludes.

II. THEORETICAL BACKGROUND

A. System Hamiltonian and observables

This section introduces the system Hamiltonian and reviews two frameworks for determining thermally averaged observables. We fix the number of particles and work in the canonical ensemble. We consider N particles with position vectors $\mathbf{r}_j$ and mass m_a in a spherically symmetric harmonic trap with angular trapping frequency ω. The model Hamiltonian $\hat{H}$ reads

$$\hat{H} = \hat{H}_0 + \hat{V}, \tag{1}$$

where

$$\hat{H}_0 = \sum_{j=1}^{N} \left(\frac{-\hbar^2}{2m_a} \nabla_j^2 + \frac{1}{2} m_a \omega^2 \mathbf{r}_j^2 \right) \tag{2}$$

denotes the noninteracting Hamiltonian. The interaction potential $\hat{V}$ reads

$$\hat{V} = \sum_{j=1}^{N} \sum_{k>j}^{N} V_{\text{tb}}^{(jk)}(r_{jk}), \tag{3}$$

where r_{jk} ($r_{jk} = |\mathbf{r}_j - \mathbf{r}_k| = |\mathbf{r}_{jk}|$) denotes the relative distance between the jth and kth particles and $V_{\text{tb}}^{(jk)}$ the interaction potential for the jth and kth particles. We employ two different interaction models. Our calculations presented in Sec. III employ the regularized zero-range Fermi-Huang pseudopotential $V_{\text{F}}^{(jk)}$ [19] with s-wave scattering length $a_s^{(jk)}$. Our PIMC calculations presented in Sec. IV employ a finite-range Gaussian potential $V_{\text{G}}^{(jk)}$, where $V_{\text{G}}^{(jk)}(r_{jk}) = U_0^{(jk)} \exp[-r_{jk}^2/(2r_0^2)]$ with depth $U_0^{(jk)}$ ($U_0^{(jk)} < 0$) and range r_0. The depth and range are adjusted so that $V_{\text{G}}^{(jk)}$ yields the desired s-wave scattering length $a_s^{(jk)}$. Throughout, we consider potentials that support at most one free-space s-wave bound state and whose range r_0 is much smaller than the characteristic harmonic trap length a_{ho}, where $a_{\text{ho}} = \sqrt{\hbar/(m_a \omega)}$.

To calculate thermally averaged quantities, we introduce the density operator $\hat{\rho}$ [12,20]:

$$\hat{\rho} = e^{-\beta \hat{H}}, \tag{4}$$

where β is the inverse temperature $\beta = 1/(k_B T)$. The expectation value for an operator $\hat{O}$ is $\text{Tr}(\hat{\rho}\hat{O})/Z$, where "Tr" stands for the trace of the matrix that is created by projecting the operator onto a complete basis set, and $Z = \text{Tr}(\hat{\rho})$ is the partition function.

A convenient basis set consists of the energy eigenstates ψ_j of the Hamiltonian $\hat{H}$. In this case, the density operator is diagonal and can be written as [12]

$$\hat{\rho} = \sum_j e^{-\beta E_j} |\psi_j\rangle \langle \psi_j|, \tag{5}$$

where E_j denotes the eigenenergy of state ψ_j, and the partition function reads

$$Z = \sum_j e^{-\beta E_j}. \tag{6}$$

The sums in Eqs. (5) and (6) are limited to the energy eigenstates ψ_j that have the proper particle statistics. For $N = 2$, e.g., the eigenstates can be grouped into states that are symmetric and those that are antisymmetric under the exchange of the two particles. If we treat two identical bosons (fermions), only the symmetric (antisymmetric) states are included in the sums in Eqs. (5) and (6). Importantly, if the complete set is known, the thermal average $\langle \hat{O} \rangle$ of the operator $\hat{O}$ can be calculated:

$$\langle \hat{O} \rangle = Z^{-1} \sum_j e^{-\beta E_j} \langle \psi_j | \hat{O} | \psi_j \rangle. \tag{7}$$

While the determination of a large number of energy eigenstates ψ_j is feasible for small systems, say $N \lesssim 4$, it becomes unfeasible for larger systems.

An alternative formulation, which forms the starting point of the PIMC approach [20] (see Sec. II C for details), projects the density operator onto the position basis $\rho_{\text{non-symm}}(\mathbf{R}, \mathbf{R}', \beta) = \langle \mathbf{R} | \hat{\rho} | \mathbf{R}' \rangle$. Here, $\mathbf{R}$ and $\mathbf{R}'$ collectively denote the position vectors $\mathbf{r}_1, \ldots, \mathbf{r}_N$ and $\mathbf{r}_1', \ldots, \mathbf{r}_N'$, respectively. The thermal average of the operator $\hat{O}$ then reads

$$\langle \hat{O} \rangle_{\text{non-symm}} = (Z_{\text{non-symm}})^{-1}$$
$$\times \int d\mathbf{R} \, d\mathbf{R}' \rho_{\text{non-symm}}(\mathbf{R}, \mathbf{R}', \beta) \langle \mathbf{R}' | \hat{O} | \mathbf{R} \rangle, \tag{8}$$

where the partition function $Z_{\text{non-symm}}$,

$$Z_{\text{non-symm}} = \int d\mathbf{R} \, \rho_{\text{non-symm}}(\mathbf{R}, \mathbf{R}, \beta), \tag{9}$$

is again the trace over the diagonal elements. To properly symmetrize or antisymmetrize the density operator, we introduce the symmetrizer $\hat{\mathcal{P}}$ [20]. For the single-component Bose and Fermi gases, $\hat{\mathcal{P}}$ can be written as [21]

$$\hat{\mathcal{P}} = \frac{1}{N!} \sum_\sigma (\pm 1)^{N_{\text{I}}(\sigma)} \hat{P}_\sigma, \tag{10}$$

where σ denotes the permutation of particle indices, $N_{\text{I}}(\sigma)$ the number of inversions in σ [22], and $\hat{P}_\sigma$ the corresponding permutation operator. For two identical fermions, e.g., $\hat{\mathcal{P}}$ reads $(1 - \hat{P}_{12})/2$, where $\hat{P}_{12}$ exchanges the particle labels 1 and 2. For mixtures, the symmetrizer $\hat{\mathcal{P}}$ has to be generalized appropriately. The partition function and thermally averaged observables then read [20]

$$Z = \int d\mathbf{R} \, \rho(\hat{\mathcal{P}}\mathbf{R}, \mathbf{R}, \beta) \tag{11}$$

and

$$\langle \hat{O} \rangle = Z^{-1} \int d\mathbf{R} \, d\mathbf{R}' \rho(\hat{\mathcal{P}}\mathbf{R}, \mathbf{R}', \beta) \langle \mathbf{R}' | \hat{O} | \mathbf{R} \rangle. \tag{12}$$

In addition to the thermally averaged energy E, this work considers a number of thermally averaged structural properties. The scaled radial density $4\pi r_j^2 \rho_{\text{rad}}(r_j)$ with normalization $4\pi \int dr_j \rho_{\text{rad}}(r_j) r_j^2 = N$ [23] tells one the likelihood of finding the jth particle at distance r_j from the trap center. The scaled pair distribution function $4\pi r_{jk}^2 P_{\text{pair}}(r_{jk})$ with normalization $4\pi \int dr_{jk} P_{\text{pair}}(r_{jk}) r_{jk}^2 = 1$ tells one the likelihood of finding

particles j and k at distance r_{jk}. The hyperradial distribution function $P_{\text{hyper}}(R)$ with normalization $\int dR \, P_{\text{hyper}}(R) = 1$ tells one the likelihood of finding particles j, k, and l in a configuration of size R; here, $R^2 = (r_{jk}^2 + r_{kl}^2 + r_{jl}^2)/3$. For $N = 3$, R is the hyperradius (see Sec. II B for details).

We also consider the condensate fraction, superfluid fraction, and superfluid density. For homogeneous systems, the condensate fraction n_c is typically defined through the large-distance behavior of the one-body density matrix for bosons and the two-body density matrix for two-component fermions [5,8]. It indicates the off-diagonal long-range order of the system. For inhomogeneous systems, the condensate fraction is defined as the largest eigenvalue of the one- and two-body density matrices for bosons and fermions, respectively [8,24,25]. Intuitively, it is clear that the long-range behavior is "cut off" by the confinement or the finite extent of the system, implying that the asymptotic behavior of the density matrix contains no information about nontrivial correlations. Section III reports the dependence of the condensate fraction n_c on the temperature for two identical bosons and two distinguishable particles. These studies extend the zero-temperature calculations of n_c presented in Ref. [26] to finite temperature. The finite-temperature behavior of n_c has previously been reported for two harmonically trapped particles in one dimension [27] but not, to the best of our knowledge, for two harmonically trapped particles in three dimensions.

The superfluid fraction n_s can be defined in various ways (see, e.g., Refs. [8,28–30] for a discussion). In this work, we utilize the moment of inertia based definition, which has its origin in the two-fluid model [31–34]:

$$n_s = 1 - \frac{I_{\text{q}}}{I_{\text{c}}}. \qquad (13)$$

The quantum moment of inertia I_{q} is defined in terms of the response to an infinitesimal rotation about the z axis,

$$I_{\text{q}} = \beta(\langle \hat{L}_{\text{tot},z}^2 \rangle - \langle \hat{L}_{\text{tot},z} \rangle^2), \qquad (14)$$

where $\hat{L}_{\text{tot},z}$ denotes the z component of the total angular momentum operator $\hat{\mathbf{L}}_{\text{tot}}$. The classical moment of inertia I_{c} is defined through

$$I_{\text{c}} = \left\langle m_{\text{a}} \sum_j r_{j,\perp}^2 \right\rangle, \qquad (15)$$

where $r_{j,\perp}$ denotes the distance of the jth particle to the z axis, $r_{j,\perp} = |\mathbf{r}_j \times \hat{z}|$. The superfluid density is defined such that $m_{\text{a}} \int d\mathbf{r} \, \rho_s(\mathbf{r}) r_\perp^2 = I_{\text{c}} - I_{\text{q}}$, where $r_\perp$ denotes the distance to the z axis [35]. The moment of inertia based definitions of the superfluid fraction and superfluid density have previously been applied to a variety of finite-sized quantum liquids [36–42]. Knowing the complete set of energy eigenstates and eigenenergies and using Eq. (7), the thermally averaged expectation values $\langle \hat{L}_{\text{tot},z} \rangle$ and $\langle \hat{L}_{\text{tot},z}^2 \rangle$ can be calculated, thereby yielding I_{q}. Within the PIMC approach, the superfluid fraction and superfluid radial density are evaluated using the area estimator [34,35,43,44] (see Sec. II C for details on the PIMC approach).

B. Efimovian states of three identical bosons in a trap

This section reviews the zero-temperature properties of three identical harmonically trapped bosons. As discussed

in the literature [6], harmonically trapped unitary Bose and Fermi gases with short-range interactions exhibit universal properties, provided the range of the interaction is smaller than all other length scales in the problem. The properties of the two-component Fermi gas near a broad s-wave resonance (and away from p- and higher-partial wave resonances) are governed by the interspecies s-wave scattering length a_s and the harmonic oscillator length a_{ho}. In the unitarity limit, i.e., for $|a_s| = \infty$, the s-wave scattering length does not define a meaningful length scale and the only remaining length scale is a_{ho} [4–6,45,46]. The corresponding energy scale is $E_{\text{ho}} = \hbar\omega$. For three or more identical bosons, an additional parameter, namely, the three-body parameter κ_*, is needed to describe the ground-state properties of the Bose gas [17,18,45,46].

The role of κ_* can be made transparent using the hyperspherical coordinate approach [6,18]. To this end, we separate off the center-of-mass motion and divide the remaining six coordinates into the hyperradius R and five hyperangles collectively denoted by Ω. In the limit of pairwise additive zero-range interactions with $1/a_s = 0$, the hyperradial and hyperangular degrees of freedom are separable [17,18,45]. The lowest eigenvalue of the hyperangular Schrödinger equation for the channel with vanishing relative angular momentum angular l is typically denoted by s_0, where $s_0 \approx 1.006\iota$ [17,18]. The hyperradial Hamiltonian $\hat{H}_R$ can then be written as

$$\hat{H}_R = \frac{-\hbar^2}{2m_{\text{a}}} \frac{\partial^2}{\partial R^2} + \frac{1}{2}m_{\text{a}}\omega^2 R^2 + \frac{\hbar^2(s_0^2 - 1/4)}{2m_{\text{a}}R^2}. \qquad (16)$$

The last term can be interpreted as an effective attractive potential, which diverges in the $R = 0$ limit. Without a three-body parameter, the system exhibits the Thomas collapse [47]. The scaled radial solution in the small-R limit is proportional to $\sqrt{R} \sin[\text{Im}(s_0) \ln R + \theta_b]$ [48], where

$$\theta_b = \arg\left(\frac{\Gamma\left(\frac{1}{2} - \frac{E_{\text{rel}}}{2E_{\text{ho}}} + \frac{s_0}{2}\right)}{\Gamma(1 + s_0)} \right) \qquad (17)$$

is the three-body phase that determines the short-range behavior of the hyperradial wave function and E_{rel} denotes the relative three-body energy. The three-body phase can be related to the three-body parameter κ_*.

Solving Eq. (17), the solid lines in Fig. 1 show the relative three-body zero-range eigenenergies as a function of the three-body phase θ_b for infinitely large s-wave scattering length. For a fixed θ_b, the energies of the negative part of the energy spectrum are spaced roughly by the factor 515 [48,49]. These geometrically spaced energy levels are the signature of the three-body Efimov effect. In free space, the spacing is exactly $\exp(2\pi/|s_0|) \approx (22.7)^2 \approx 515$ and the three-body parameter κ_* is defined as the binding momentum of one of the Efimov trimers, $E_{\text{rel}} = \hbar^2\kappa_*^2/m$ [18]. Knowing κ_*, the ratio between consecutive energy levels of the free-space system is fixed. For the trapped system, corrections arise when the trimer size approaches the harmonic oscillator length. For the states with positive energy, the spacing between consecutive states is approximately $2E_{\text{ho}}$ [48–50].

We now connect the energy spectrum for the Gaussian interaction model V_{G} with that for the zero-range model. In free space, the three-body system with pairwise Gaussian interaction supports infinitely many states. The spacing between the
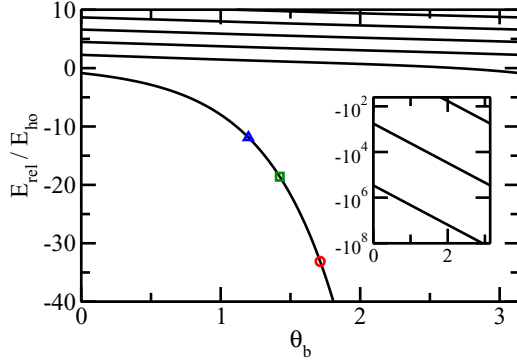
FIG. 1. (Color online) Relative energy spectrum as a function of the three-body phase θ_b for three identical bosons in a harmonic trap interacting through zero-range potentials with infinite s-wave scattering lengths. The circle, square, and triangle show the ground-state energy for the Gaussian two-body interaction with range $r_0/a_{\mathrm{ho}} = 0.06, 0.08$, and 0.1, respectively. The inset shows the negative energy regime on a log scale. The spacing between the energy levels for fixed θ_b is very close to 515, i.e., very close to the free-space scaling factor.

ground state and the first excited state at unitarity is $(22.98)^2$ and between the energies of the first excited state and the second excited state is $(22.7)^2$. These values are close to the universal scaling factor. Indeed, the Gaussian interaction model has been used extensively in the literature to describe Efimov physics [51–53]. For the trapped system, the ratio between the range r_0 of the two-body interaction and the harmonic oscillator length comes into play. The circle, square, and triangle in Fig. 1 show the relative energy of the lowest state of the trapped system for $r_0/a_{\mathrm{ho}} = 0.06, 0.08$, and 0.1, respectively. Assuming that the zero-range energy spectrum provides a reasonable description, Fig. 1 allows us to estimate the three-body phase.

For our purposes, the size of the trimer compared to the range of the interaction is relevant. For the three r_0 considered, the size of the lowest trimer, as measured by the expectation value of the hyperradius R, is roughly $0.160a_{\mathrm{ho}}$, $0.212a_{\mathrm{ho}}$, and $0.266a_{\mathrm{ho}}$, i.e., the trimers are much smaller than a_{ho}, and thus very close to the free-space trimers. The lowest Efimov trimer is only a bit larger than r_0 (the size is about $2.66r_0$ for all cases), implying that we expect finite-range effects to be non-negligible. Indeed, Fig. 2 shows that the hyperradial densities of the lowest state of the finite-range three-body system (solid and dotted lines) differ notably from the hyperradial density of the zero-range system (dashed line). This difference cannot be attributed to the fact that the hyperradial densities are calculated at finite temperature (the finite-range $T = 0$ hyperradial densities are, on the scale chosen, indistinguishable from those shown in Fig. 2) but is due to finite-range effects. Despite these finite-range corrections, the Gaussian interaction model allows us to gain insights into finite-temperature effects that are governed by the lowest Efimov state of the three-body system (see Sec. IV for details).

C. PIMC approach

This section reviews the finite-temperature continuous-space PIMC approach [20]. The key idea behind the PIMC approach is to convert the calculations at low temperature
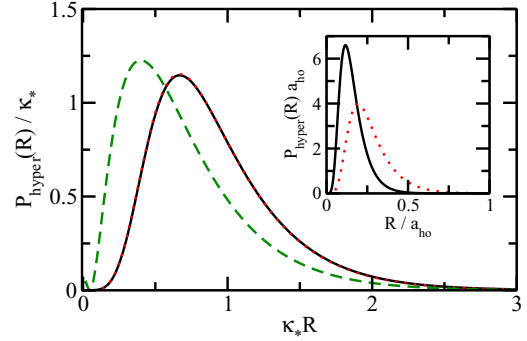

FIG. 2. (Color online) Hyperradial density $P_{\mathrm{hyper}}(R)$ for three identical bosons at unitarity. Solid and dotted lines show the PIMC results at $k_B T/E_{\mathrm{ho}} = 0.4$ for the Gaussian model potential with $r_0/a_{\mathrm{ho}} = 0.06$ and 0.1, respectively (in the main panel, the curves are indistinguishable on the scale shown). The main panel and the inset show the same data but use a different scaling: The main panel uses units derived from the energy of the three-boson system at $T = 0$, while the inset employs harmonic oscillator units. For comparison, the dashed line shows the hyperradial density obtained using the zero-range pseudopotential with κ_* determined by the relative energy of the finite-range potential.

(large β) into a series of calculations at high temperature. Specifically, the PIMC approach rewrites $\exp(-\beta \hat{H})$ in terms of the product $\prod_{j=1}^{M} \exp(-\tau \hat{H})$, where $\tau = \beta/M$. The idea is to use a sufficiently small τ (sufficiently large integer M) so that the integrals involving τ can be factorized with controllable error. In the calculations reported in Sec. IV, we use $M \approx 400$–7000 (the actual number used depends on the temperature T and the two-body range r_0). Inserting $\int_j |\mathbf{R}_j\rangle\langle\mathbf{R}_j|$ repeatedly, Eq. (12) becomes [20]

$$
\langle \hat{\mathcal{O}} \rangle = Z^{-1} \int d\mathbf{R}_0 \ldots d\mathbf{R}_M \rho(\hat{\mathcal{P}}\mathbf{R}_0, \mathbf{R}_1, \tau)
$$
$$
\times \rho(\mathbf{R}_1, \mathbf{R}_2, \tau) \times \cdots \times \rho(\mathbf{R}_{M-1}, \mathbf{R}_M, \tau)\langle\mathbf{R}_M \mid \mathcal{O} \mid \mathbf{R}_0\rangle.
$$
$$(18)$$

To evaluate expectation values of operators that probe the diagonal but not the off-diagonal elements of the real-space density matrix, only closed paths with $\hat{\mathcal{P}}\mathbf{R}_0 = \mathbf{R}_M$ are needed. The density matrix $\rho(\mathbf{R}_{j-1}, \mathbf{R}_j, \tau)$ is, in general, unknown. Using the second- or fourth-order factorization [20,54,55], the high-temperature density operator can be divided into the noninteracting and interacting parts

$$
\exp[-\tau(\hat{H}_0 + \hat{V})]
$$
$$
= \exp\left(-\tau\frac{\hat{V}}{2}\right)\exp(-\tau\hat{H}_0)\exp\left(-\tau\frac{\hat{V}}{2}\right) + \cdots \quad (19)
$$

and

$$
\exp[-\tau(\hat{H}_0 + \hat{V})]
$$
$$
= \exp\left(-\tau\frac{\hat{V}}{6}\right)\exp\left(-\tau\frac{\hat{H}_0}{2}\right)\exp\left(-\tau\frac{2\tilde{V}}{3}\right)
$$
$$
\times \exp\left(-\tau\frac{\hat{H}_0}{2}\right)\exp\left(-\tau\frac{\hat{V}}{6}\right) + \cdots, \quad (20)
$$

where $\tilde{V}$ is given by $\hat{V} + \tau^2[\hat{V},[\hat{H}_0,\hat{V}]]/48$. For observables that are determined by the diagonal elements of the density matrix, these factorizations yield errors that scale as τ^3 and τ^5, respectively [54]. The noninteracting part of the density matrix in the position basis can be written compactly as [12,56]

$$\langle \mathbf{R}|e^{-\tau \hat{H}_0}|\mathbf{R}'\rangle = a_{\text{ho}}^{-3N}[2\pi \sinh(\tilde{\beta})]^{-3N/2}$$
$$\times \exp\left[-\frac{(\mathbf{R}^2 + \mathbf{R}'^2)\cosh(\tilde{\beta}) - 2\mathbf{R}\cdot\mathbf{R}'}{2\sinh(\tilde{\beta})a_{\text{ho}}^2}\right]. \quad (21)$$

Here, $\tilde{\beta}$ denotes the dimensionless inverse temperature $\tilde{\beta} = \beta E_{\text{ho}}$. The potential dependent part of the density matrix reduces to evaluating the potential at the given configuration.

The energy and structural expectation values are calculated following standard procedures [20]. The superfluid fraction is calculated using the area estimator [20,34,43]. The superfluid density is calculated following Ref. [35]. The condensate fraction requires off-diagonal elements of the density matrix, i.e., open paths [57]. We have not yet implemented this.

In the high-temperature limit, the particle statistics becomes negligible and the system behaves, to leading order, as a noninteracting gas of Boltzmann particles. To analyze the effects of the particle statistics for systems with two or more identical particles in the low-temperature regime, we find it useful to divide the partition function Z into "even" and "odd" contributions (a closely related definition can be found in Ref. [58]):

$$Z = Z_{\text{even}} \pm Z_{\text{odd}}, \quad (22)$$

where

$$Z_{\text{even}} = \sum_{P_{\text{even}}} \int d\mathbf{R}\, \rho(\hat{\mathcal{P}}\mathbf{R},\mathbf{R},\beta) \quad (23)$$

and

$$Z_{\text{odd}} = \sum_{P_{\text{odd}}} \int d\mathbf{R}\, \rho(\hat{\mathcal{P}}\mathbf{R},\mathbf{R},\beta); \quad (24)$$

the plus and minus signs apply if the system contains identical bosons and fermions, respectively (here and in the remainder of this section we assume that the system contains only one type of identical particles). The sum over P_{even} includes the permutations that are characterized by even $N_{\text{I}}(\sigma)$ and the sum over P_{odd} includes the permutations that are characterized by odd $N_{\text{I}}(\sigma)$. The sum over P_{odd} is only nonzero if the system under study contains two or more identical particles. When the temperature is high, only the identity permutation (and thus only the first term) contributes, i.e., the statistics is suppressed and the system behaves like a Boltzmann gas. As the temperature decreases, the relative importance of the second term increases. In the zero-temperature limit, the two terms contribute equally. We define the statistical factor S as the normalized ratio of the "even" and "odd" partition functions [58,59]:

$$S = \frac{Z_{\text{even}} - Z_{\text{odd}}}{Z_{\text{even}} + Z_{\text{odd}}}. \quad (25)$$

The statistical factor S approaches 1 in the high-temperature limit and 0 in the zero-temperature limit. Since the partition
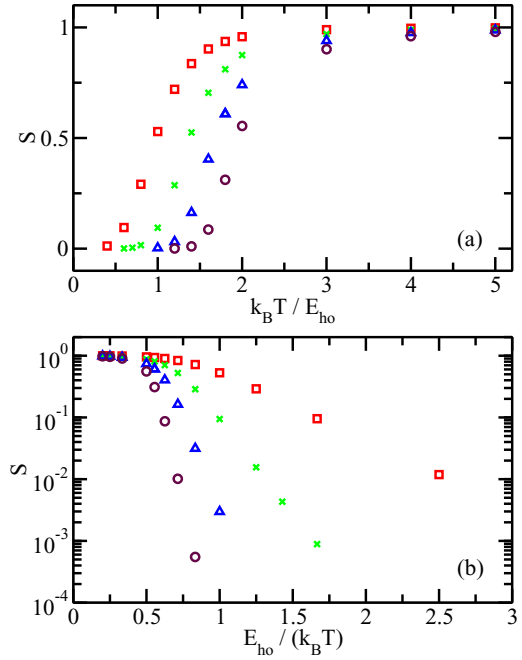

FIG. 3. (Color online) Statistical factor S for the $(N-1,1)$ system with interspecies potential V_G with $r_0 = 0.06a_{\text{ho}}$ and $1/a_s = 0$. Squares, crosses, triangles, and circles show the statistical factor S as a function of (a) the temperature T and (b) the inverse temperature T^{-1} for $N = 3,4,5,$ and 6, respectively.

function enters into the denominator of the thermal expectation values, the statistical factor characterizes the numerical demands on the simulation for systems with identical fermions. The smaller S is, the harder the simulation is. As a rule of thumb, if we compare the S value for the same system at two different temperatures, then the simulation time required to obtain comparable accuracy for the observables at the two temperatures is $(S_{\text{high}}/S_{\text{low}})^2$ times larger at the lower temperature than at the higher temperature (here, S_{high} and S_{low} are the S values at the higher and lower temperature, respectively). This phenomenon is known as the Fermi sign problem [58,60–62]. A related interpretation of S is in terms of the "quantum statistics" of the system under study. For both bosons and fermions, a value of S around 1 indicates that the particles approximately follow Boltzmann statistics while a value of S close to 0 indicates that exchange effects play an important role.

Figure 3(a) shows the statistical factors as a function of the temperature for the N-particle system consisting of $N-1$ identical particles and one impurity. The identical particles do not interact while the unlike particles interact through a Gaussian potential with $r_0 = 0.06a_{\text{ho}}$ and infinite s-wave scattering length. The statistical factor deviates notably from one when the temperature is of the order of the "Fermi temperature" or lower. The Fermi temperature is equal to $5E_{\text{ho}}/2$ to $7E_{\text{ho}}/2$ for the $(N-1,1)$ systems with $N = 3$–6. At low temperature, the statistical factor depends exponentially on the inverse temperature, i.e., $S \propto \exp(-\beta\alpha_N)$ [58], where α_N increases faster than linear with increasing N. We have performed reliable calculations for the symbols shown in Fig. 3. The lowest temperature that can be reached depends, of course, on the available computational resources. However,

since the Fermi sign problem increases exponentially with decreasing temperature, the lower-T limit shown in Fig. 3 is somewhat generic. The physics of the $(N-1,1)$ systems with Bose, Fermi, and Boltzmann statistics is discussed in more detail in Sec. IV B.

III. CONDENSATE AND SUPERFLUID FRACTIONS OF THE TWO-BODY SYSTEM

The condensate and superfluid fractions are distinct physical quantities that vanish when the de Broglie wavelength is small but differ from zero when the de Broglie wavelength is large. This section compares the condensate and superfluid fractions for the simplest interacting system, namely, for two particles in a harmonic trap with zero-range s-wave interactions. For this system, the eigenspectrum and eigenfunctions are known in compact analytical form [63], which facilitates the calculation of n_c and n_s over a wide temperature range. The superfluid fraction is calculated using the energy eigenstates in the moment of inertia based definition [see Eq. (13)].

An important point of this section is that the superfluid and condensate fractions are meaningful quantities not just for large systems but also for small systems. We will show in Sec. IV A that the superfluid fraction of the N boson system is, for certain parameter combinations, approximated well by that of a single particle. The superfluid fraction reflects symmetry properties of the system [30,64,65]. The connection between superfluidity and angular momentum decoupling mechanisms, e.g., has been discussed in some detail in the context of small doped bosonic helium droplets [66,67]. The condensate fraction is given by the largest eigenvalue of the one-body reduced density matrix $\rho_{\rm red}$ or, equivalently, the largest occupation number of the natural orbitals [8,24,25]. Since the natural orbitals are defined by decomposing the reduced density matrix in a specific way, the occupation numbers, and hence the condensate fraction, can be interpreted as a particular measure of the particle-particle correlations of the system. Our approach for determining the finite-temperature reduced density matrix of the two-body system (which is discussed in the following paragraphs) also allows one to determine entanglement measures such as the concurrence [68] and negativity [69] of the two-particle system over a wide temperature range. Such calculations appear to have been challenging in the past [70].

The reduced density matrix $\rho_{\rm red}$ for the two-particle system reads

$$\rho_{\rm red}(\mathbf{r}'_1,\mathbf{r}_1,\beta) = Z^{-1} \int d\mathbf{r}_2 \rho(\mathbf{r}'_1,\mathbf{r}_2,\mathbf{r}_1,\mathbf{r}_2,\beta). \quad (26)$$

Using the separation of the center-of-mass and relative coordinates, Eq. (26) becomes

$$\rho_{\rm red}(\mathbf{r}'_1,\mathbf{r}_1,\beta)$$
$$= Z^{-1} \int d\mathbf{r}_2 \rho_{\rm rel}(\mathbf{r}'_{\rm rel},\mathbf{r}_{\rm rel},\beta)\rho_{\rm c.m.}(\mathbf{r}'_{\rm c.m.},\mathbf{r}_{\rm c.m.},\beta), \quad (27)$$

where $\mathbf{r}_{\rm rel} = \mathbf{r}_1 - \mathbf{r}_2$, $\mathbf{r}'_{\rm rel} = \mathbf{r}'_1 - \mathbf{r}_2$, $2\mathbf{r}_{\rm c.m.} = \mathbf{r}_1 + \mathbf{r}_2$, $2\mathbf{r}'_{\rm c.m.} = \mathbf{r}'_1 + \mathbf{r}_2$,

$$\rho_{\rm rel}(\mathbf{r}'_{\rm rel},\mathbf{r}_{\rm rel},\beta)$$
$$= \sum_{ilm} e^{-\beta E_{i,l}} \psi^*_{ilm}(\mathbf{r}'_{\rm rel})\psi_{ilm}(\mathbf{r}_{\rm rel}), \quad (28)$$

and

$$\rho_{\rm c.m.}(\mathbf{r}'_{\rm c.m.},\mathbf{r}_{\rm c.m.},\beta)$$
$$= \sum_{QLM} e^{-\beta E_{Q,L}} \psi^*_{QLM}(\mathbf{r}'_{\rm c.m.})\psi_{QLM}(\mathbf{r}_{\rm c.m.}). \quad (29)$$

In Eq. (29), $E_{Q,L}$ denotes the center-of-mass eigenenergy, which can be conveniently written in terms of the principal quantum number Q ($Q = 0,1,\ldots$) and the center-of-mass angular momentum quantum number L ($L = 0,1,\ldots$), $E_{Q,L} = (2Q+L+3/2)E_{\rm ho}$. The energies are independent of the projection quantum number M ($M = -L,-L+1,\ldots,L$). In Eq. (28), $E_{i,l}$ denotes the relative eigenenergy. For two Boltzmann particles, all l values are allowed. For two identical bosons, in contrast, only even l values are allowed. For finite relative angular momentum l, the relative energy reads $E_{i,l} = (2i+l+3/2)E_{\rm ho}$, where $i = 0,1,\ldots$. For $l = 0$, i denotes a noninteger quantum number whose values are determined semianalytically by solving a transcendental equation [63]. As in the center-of-mass case, the relative energies are independent of the projection quantum number m ($m = -l,-l+1,\ldots,l$).

To evaluate $\rho_{\rm rel}$, we use the fact that the $l > 0$ states are not affected by the zero-range interactions and write $\rho_{\rm rel} = \rho_{\rm rel}^{l>0,\rm NI} + \rho_{\rm rel}^{l=0,\rm int}$, where $\rho_{\rm rel}^{l>0,\rm NI}$ denotes the $l > 0$ contributions to the density matrix (these contributions are independent of the s-wave scattering length) and $\rho_{\rm rel}^{l=0,\rm int}$ the $l = 0$ contribution that depends on a_s. To evaluate the latter, it is convenient to project the interacting $l = 0$ energy eigenstates onto the noninteracting harmonic oscillator states $\psi_{i00}(\mathbf{r}_{\rm rel}) = \sum_{q=0}^{\infty} C_q^{(i)} \psi_{q00}(\mathbf{r}_{\rm rel})$, where $q = 0,1,\ldots$. The expansion coefficients $C_q^{(i)}$ are known analytically [26,63]. Now that $\rho_{\rm c.m.}$ and $\rho_{\rm rel}$ are expressed in terms of the noninteracting wave functions in the relative and center-of-mass coordinates, the integral over $d\mathbf{r}_2$ can be performed by reexpressing, using the Talmi-Moshinsky brackets [71,72], the harmonic oscillator eigenstates in the relative and center-of-mass coordinates in terms of the harmonic oscillator eigenstates in the single-particle coordinates. After integrating over $d\mathbf{r}_2$, we project the reduced density matrix onto single-particle states in the $\mathbf{r}_1$ coordinate. Using the orthogonality of the Clebsch-Gordon coefficients as well as other standard identities from angular momentum algebra, the calculation of the matrix elements simplifies dramatically. The resulting one-body density matrix is found to be block diagonal in the l and m quantum numbers. Furthermore, since the lowest $l = 0$ state always minimizes the energy, the largest occupation number comes from the $(l,m) = (0,0)$ submatrix. The results discussed in the following are obtained by diagonalizing a 20×20 submatrix. Increasing the matrix size to 50×50 changes the results by less than 1%.

The main panel of Fig. 4(a) shows the condensate fraction n_c for two Boltzmann particles as a function of the temperature for various s-wave scattering lengths a_s. Solid, dotted, dashed, dash-dotted, dash-dot-dotted, and dash-dash-dotted lines are for $a_{\rm ho}/a_s = -\infty,-2,-1,0,1$, and 2, respectively. As the temperature increases, the condensate fraction n_c decreases for all interaction strengths. At zero temperature, n_c decreases as the inverse scattering length increases. At finite temperature, however, we observe in some
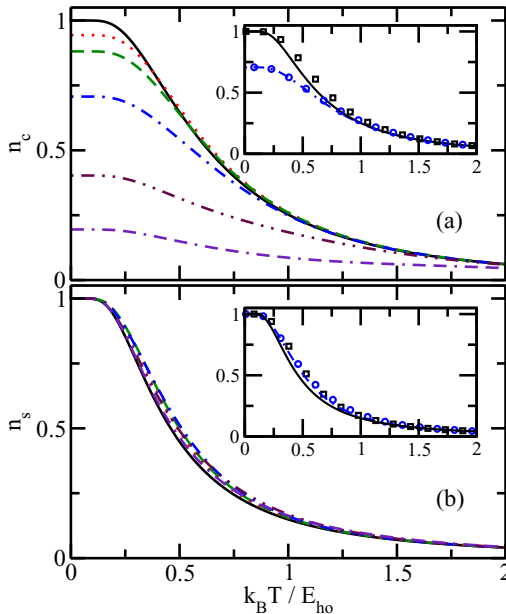
FIG. 4. (Color online) The lines show (a) the condensate fraction n_c and (b) the superfluid fraction n_s as a function of the temperature T for two Boltzmann particles with zero-range interaction for various a_s. The solid, dotted, dashed, dash-dotted, dash-dot-dotted, and dash-dash-dotted lines are for $a_{ho}/a_s = -\infty, -2, 1, 0, 1$, and 2, respectively. In panel (b), the dependence on a_s is small. The insets compare (a) the condensate fraction n_c and (b) the superfluid fraction n_s for two Boltzmann particles (lines; these are the same data as shown in the main parts of the figure) and two identical bosons (squares and circles correspond to $a_{ho}/a_s = -\infty$ and 0, respectively) as a function of the temperature.

cases [see the $k_B T \approx E_{ho}/2$ to E_{ho} regime in Fig. 4(a)] that the condensate fraction increases slightly as $|a_s|$ ($a_s < 0$) increases. This is caused by the interplay of the interaction energy and the temperature-dependent Boltzmann weight.

The condensate fraction for two identical bosons is very similar to that for two Boltzmann particles. The inset of Fig. 4(a) compares the condensate fraction for two identical bosons (symbols) with those for two Boltzmann particles (lines) for $a_{ho}/a_s = -\infty$ and 0, respectively. It can be seen that the condensate fraction for two identical bosons falls off slightly slower with increasing temperature than that for two Boltzmann particles. This is because the Bose statistics excludes the states with odd relative angular momentum l, implying that the $l = 0$ states (which are responsible for the nonzero condensate fraction) are relatively more important for two identical bosons than for two Boltzmann particles.

For comparison, Fig. 4(b) shows the superfluid fraction n_s for two Boltzmann particles for the same scattering lengths. The superfluid fraction n_s depends weakly on the s-wave scattering length. Specifically, the superfluid fraction approaches 1 in the low-temperature regime for all s-wave scattering lengths. This is a consequence of the fact that the lowest-energy eigenstate has vanishing total orbital angular momentum for all s-wave scattering lengths. The inset of Fig. 4(b) compares the superfluid fraction for two Boltzmann particles (lines) with those for two identical bosons (symbols).

As in the case of the condensate fraction, the switch from Boltzmann to Bose statistics changes the superfluid fraction only by a small amount.

A comparison of Figs. 4(a) and 4(b) shows that the condensate and superfluid fractions are distinctly different quantities. When the two-body system forms a molecule (for positive a_s), the condensate fraction is small. The superfluid fraction, in contrast, remains approximately 1 in the low-temperature regime, indicating that the response to an infinitesimal rotation is largely independent of the size of the system (the density decreases with increasing $1/a_s$) and instead largely determined by its spherical shape.

Next, we consider two identical fermions. Naively, this system might be thought to be "uninteresting" since the Pauli exclusion principle prohibits scattering in the s-wave channel. As we show now, two noninteracting identical fermions display intriguing temperature-dependent behaviors. For two identical noninteracting fermions, the condensate fraction equals $1/2$ at $T = 0$ and decreases monotonically. The superfluid fraction displays [see Fig. 5(c)] a nonmonotonic dependence on the temperature. As expected, n_s is zero in the high-T limit, increases to around 0.2 at $k_B T = E_{ho}/2$, and then diverges to $-\infty$ in the zero-temperature limit. As discussed in Ref. [65], this behavior can be understood by analyzing the classical moment of inertia I_c and the quantum moment of inertia I_q [see the Figs. 5(d) and 5(e), respectively]. Specifically, the fact that the lowest-energy eigenstate has $L_{tot} = 1$ is responsible for the increase of I_q at low temperature. Motivated by the nuclear physics literature [73,74], we refer to this behavior as "abnormal."

The fact that the superfluid fraction for two identical fermions becomes negative in the low-temperature regime can be understood as follows [65]. Two identical bosons at low temperature do not respond to an infinitesimal external rotation ($n_s \to 1$ as $T \to 0$) since the lowest-energy eigenstate has $L_{tot} = 0$. Two identical fermions at low temperature, however, do respond to an infinitesimal external rotation ($n_s \to -\infty$ as $T \to 0$) since the lowest-energy eigenstate has $L_{tot} = 1$. The physical picture is that the system "speeds up" faster than we would expect for a normal fluid with the same classical moment of inertia [65].

To gain further insight into the superfluid properties of the fermionic system, we analyze the radial and superfluid densities. The radial densities for particles 1 and 2 are identical and the subscript j of r_j will be dropped in what follows. Solid, dotted, and dashed lines in Fig. 5(a) show the scaled radial density $4\pi \rho_{rad}(r)r^2$ for $k_B T/E_{ho} = 0.5, 0.264\,59$, and 0.2, respectively. The radial density is fairly insensitive to the temperature. The radial superfluid density [see Fig. 5(b)], in contrast, changes notably with the temperature. This is not unexpected since the superfluid fraction varies strongly in the low-temperature regime. The radial superfluid density takes negative values near the trap center and positive values near the edge of the cloud. The oscillation of the radial superfluid density reflects the fact that the lowest-energy eigenstate has total angular momentum quantum number $L_{tot} = 1$. For large r, the probability of finding two particles close to each other is extremely low. This translates into the Fermi statistics playing a negligible role. On the other hand, we expect that the Fermi statistics is much more important near the trap
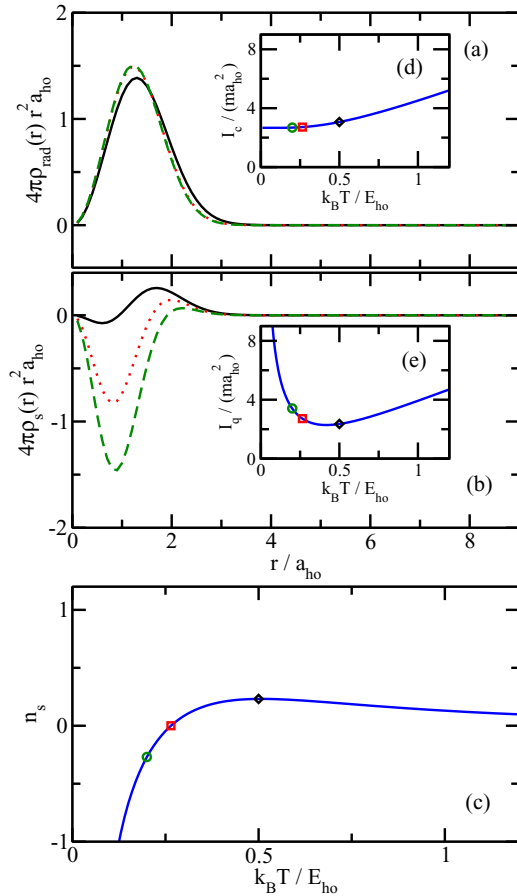
FIG. 5. (Color online) Panels (a) and (b) show radial densities for two identical noninteracting fermions. Solid, dotted, and dashed lines show (a) the scaled radial total density and (b) the scaled radial superfluid density, for $k_B T/E_{\rm ho} = 0.5, 0.264\,59$, and 0.2, respectively. In panel (a), the dotted line is hardly distinguishable from the dashed line. The solid lines in panels (c)–(e) show (c) the superfluid fraction n_s, (d) the classical moment of inertia $I_{\rm c}$, and (e) the quantum mechanical moment of inertia $I_{\rm q}$ as a function of the temperature T. The diamond, square, and circle mark the temperatures considered in panels (a) and (b).

center. In the language of path integrals, the "permuted paths" (i.e., the paths that come from exchanging particles 1 and 2 and thus contribute with a negative sign to the partition function) are largely concentrated near the center. These "permuted paths" contribute negatively to the area estimator and span larger areas compared to the "unpermuted paths." As a consequence, the superfluid density is negative near the trap center.

The analysis presented here for two noninteracting identical fermions can be extended to two-component Fermi gases with interspecies s-wave interactions consisting of $N = 3$ or more particles. Selected results were presented in our earlier work [65]. We anticipate that the analysis of the superfluid properties presented in the previous paragraphs for two noninteracting fermions will inspire other studies, for bosons or fermions, that are concerned with understanding the distribution of the superfluid properties in finite-sized systems or systems with interfaces [35,39–42,66,75–77].
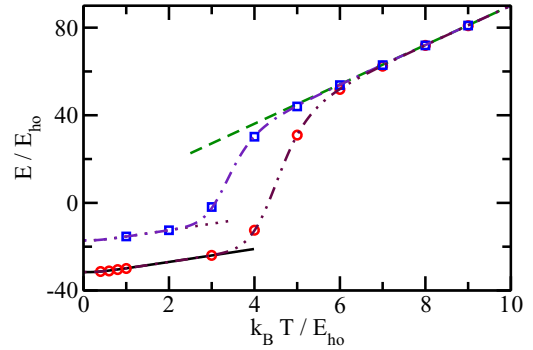

FIG. 6. (Color online) Energies as a function of the temperature T for three identical bosons at unitarity interacting through $V_{\rm G}$ with different r_0. Circles and squares show the PIMC results for $r_0/a_{\rm ho} = 0.06$ and 0.08, respectively. For comparison, the solid and dotted lines show the result obtained using the droplet state plus center-of-mass excitations. The dashed line shows the thermally averaged energy for three identical noninteracting bosons. Dash-dot-dotted and dash-dotted lines show results obtained using the simple combined model for $r_0/a_{\rm ho} = 0.06$ and 0.08 (see the text for discussion).

IV. N-BODY SYSTEMS

A. N identical bosons

This section discusses the temperature-dependent properties of N identical bosons under external spherically symmetric harmonic confinement interacting through the Gaussian model potential $V_{\rm G}$ with infinite s-wave scattering length. Circles and squares in Fig. 6 show the energy of the three-boson system, obtained from the PIMC simulations, as a function of the temperature for $r_0/a_{\rm ho} = 0.06$ and 0.08, respectively. For both ranges, the energy shows three distinct regions. The energy increases approximately linearly at small T, turns up relatively sharply around $k_B T = 4E_{\rm ho}$ or $3E_{\rm ho}$, and then changes again linearly. The energy at low temperature, if expressed in harmonic oscillator units, shows a strong range dependence. The energy at high temperature, in contrast, is to leading order independent of r_0. We refer to the rapid change of the energy from one approximately linear regime to the other approximately linear regime as a phase-transition-like feature.

We now introduce a simple parameter-free model that reproduces the energy curves semiquantitatively (see the dash-dot-dotted and dash-dotted lines in Fig. 6). The assumptions going into the model are that the low-temperature behavior is governed by the properties of the lowest Efimov trimer and that the high-temperature behavior is governed by the properties of the noninteracting three-boson gas. Treating only the lowest Efimov trimer state and its center-of-mass excitations, we obtain the solid and dotted lines in Fig. 6 for $r_0/a_{\rm ho} = 0.06$ and 0.08, respectively. These thermally averaged energies are obtained using the lowest eigenenergy of the trapped three-boson system, i.e., using the eigenenergy of the state that shows Efimov characteristics, and summing over the center-of-mass excitations. The dashed line shows the thermally averaged energy of three noninteracting identical bosons. If we combine these two limiting behaviors, the model partition function $Z_{\rm model}$ reads

$$Z_{\rm model}(\beta) = Z_{\rm droplet}(\beta) + Z_{\rm gas}(\beta), \qquad (30)$$

where $Z_{\text{droplet}}(\beta) = z(\beta) \exp(-\beta E_{\text{droplet}})$ and $Z_{\text{gas}}(\beta) = [z^3(\beta) + 3z(2\beta)z(\beta) + 2z(3\beta)]/6$. Here, E_{droplet} denotes the lowest relative eigenenergy of the three-boson system and $z(\beta)$ the partition function of a single harmonically trapped particle. The second and third terms in Z_{gas} originate from the symmetrization of Z_{gas}. The resulting energies are shown in Fig. 6 by the dash-dot-dotted and dash-dotted lines for $r_0/a_{\text{ho}} = 0.06$ and 0.08, respectively. The agreement between this simple combined model and the PIMC calculations is very good.

One may ask why the simple combined model works so well. We attribute this to primarily two things. First, for the examples shown in Fig. 6, the energy separation between the lowest Efimov trimer state and the gaslike states is large (the case where $|E_{\text{droplet}}|$ is not much larger than E_{ho} is briefly discussed at the end of this section). Second, although the system is strongly interacting, the noninteracting Bose gas model describes the density of states approximately correctly. The reason is that a significant fraction of the states is not affected by the s-wave interactions [45]. In fact, if we replace the partition function Z_{gas} for the noninteracting Bose gas by the partition function for the noninteracting Boltzmann gas, then the model predicts that the energy changes rapidly at a lower temperature than predicted by the PIMC results. If, on the other hand, we replace the partition function Z_{gas} for the noninteracting Bose gas by a partition function for three identical bosons that accounts for the s-wave interactions in an approximate manner (we reduce the energy of all states that are affected by the s-wave interactions by E_{ho}), the resulting energy curves are, on the scale of Fig. 6, indistinguishable from the dash-dot-dotted and dash-dotted curves.

Circles and squares in Fig. 7(a) show the thermally averaged PIMC energies for the Gaussian model interaction with $r_0/a_{\text{ho}} = 0.1$ and $1/a_s = 0$ for $N = 3$ and 4, respectively. As the three-boson system, the four-boson system displays a "phase-transition-like" feature. To model four- and higher-body boson systems, we generalize the combined model introduced above as follows. In Eq. (30), $Z_{\text{droplet}}(\beta)$ now denotes the partition function determined by the lowest N-boson energy state plus center-of-mass excitations and $Z_{\text{gas}}(\beta)$ denotes the partition function of the noninteracting N-boson gas. As above, Z_{gas} is properly symmetrized. The solid line in Fig. 7(a) shows the resulting energy for the four-boson system. The agreement with the PIMC results is good. It should be noted that the combined model neglects, for systems with $N > 3$, a large number of states. For example, for the four-boson system, it neglects the excited four-boson Efimov state whose energy is, in the universal regime, 1.002 times the trimer energy [78] as well as "atom-trimer states" that can be approximately described as consisting of an Efimov trimer with the fourth particle occupying one of the harmonic oscillator states. These states contribute relatively little to the partition function for two reasons. First, the separation between the four-body ground-state energy and the energy of the excited tetramer and the separation between the four-body ground-state energy and the atom-trimer states is large (the factor for the former is 4.61 in the universal regime [78]). Second, the density of states of the atom-trimer states is negligible compared to the density of states of the gaslike boson-boson-boson-boson states. We conjecture that
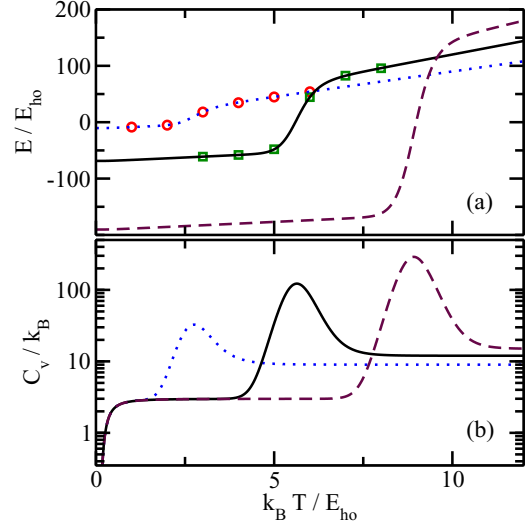

FIG. 7. (Color online) Phase-transition-like feature for N identical harmonically trapped bosons interacting through V_G with $1/a_s = 0$. (a) Circles and squares show the energy obtained by the PIMC approach for $r_0 = 0.1 a_{\text{ho}}$ and $N = 3$ and 4, respectively, as a function of the temperature T. The dotted, solid, and dashed lines show the energies for $N = 3$, 4, and 5 obtained using the simple combined model. (b) The dotted, solid, and dashed lines show the heat capacity C_v for $N = 3$, 4, and 5, respectively, as a function of T.

the combined model also provides a good description for larger Bose systems. We stress that the combined model is fully analytical, provided that the eigenenergy of the lowest N-body state, which can be considered as being tied to the lowest trimer eigenstate, is known. The dashed line in Fig. 7(a) shows the energy for $N = 5$ bosons interacting through V_G with $r_0/a_{\text{ho}} = 0.1$ and $1/a_s = 0$ as a function of the temperature. This curve is obtained using the combined model with the eigenenergy of the lowest $N = 5$ energy eigenstate as input (see Table I for the energy).

Figure 7(a) shows that the phase-transition-like feature for fixed r_0 moves to higher temperature with increasing N. To estimate the transition temperature T_{tr}, we calculate the heat capacity C_v, $C_v = \partial E/\partial T$. The dotted, solid, and dashed lines in Fig. 7(b) show C_v, obtained using the combined model for

TABLE I. Relative zero-temperature energy E_{droplet} for N bosons interacting through the Gaussian potential V_G with diverging s-wave scattering length. The energies in columns 2 and 5 are obtained by extrapolating the PIMC results to $T = 0$. The energies are expressed in units of the short-range energy scale E_{sr}, $E_{\text{sr}} = \hbar^2/(mr_0^2)$. Column 3 reports the energies from Ref. [79]; no error bars are reported in that reference. For comparison, our basis-set expansion approach (see Ref. [80] for a discussion of the approach) yields $E_{\text{droplet}}/E_{\text{sr}} = -0.119\,23(1)$ and $-0.701\,73(5)$ for $N = 3$ and 4, respectively.

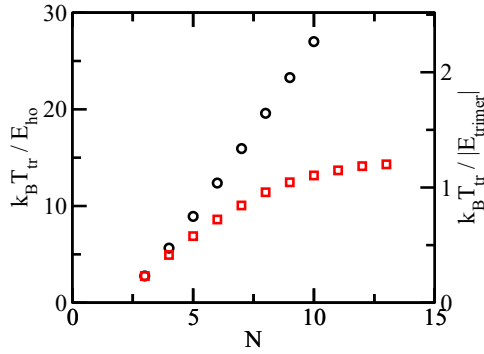| N	$E_{\text{droplet}}/E_{\text{sr}}$	E_a/E_{sr}	N	$E_{\text{droplet}}/E_{\text{sr}}$
3		-0.1191	7	$-6.544(11)$
4	$-0.700(4)$	-0.70	8	$-10.075(16)$
5	$-1.9127(5)$	-1.92	9	$-14.48(2)$
6	$-3.839(6)$	-3.84	10	$-19.76(4)$

FIG. 8. (Color online) Transition temperature T_{tr} for N identical bosons in a harmonic trap at unitarity as a function of N. The transition temperature is calculated using the simple combined model. The circles show T_{tr} using the droplet energies for the Gaussian two-body interaction model employed in this work. For comparison, the squares show T_{tr} using the droplet energies for a model Hamiltonian with attractive two-body and repulsive three-body interactions [53] (to obtain the squares, the three-body eigenenergy $E_{droplet} = E_{trimer}$ is chosen such that it agrees with that for the Gaussian two-body interaction model, i.e., the circle and the square agree for $N = 3$).

the thermally averaged energy [see lines in Fig. 7(a)], as a function of the temperature for $N = 3$, 4, and 5, respectively. The heat capacity curves show distinct maxima. We define the transition temperature T_{tr} as the temperature at which the heat capacity takes on its maximum.

The circles in Fig. 8 show the transition temperature for N bosons interacting through V_G with $r_0/a_{ho} = 0.1$ and $1/a_s = 0$ as a function of N. To obtain the transition temperature, we extrapolate the PIMC energies at low temperature to the zero-temperature limit. The resulting zero-temperature energies $E_{droplet}$ are reported in Table I. We find that the energy $E_{droplet}$ scales with the number of pairs, i.e., as $N(N-1)/2$. This implies that the transition temperature increases linearly with increasing N.

Since the N-body droplet states are only somewhat larger than r_0, the Gaussian interaction model employed in our work suffers from finite-range effects and provides only an approximate description of the N-body Efimov scenario. Note that the recent work by Gattobigio and Kievsky [79] suggests a means to correct for these finite-range effects. Here, we pursue a different approach. To see how the transition temperature changes when the droplet energies scale to leading order linearly with N, which is one of the scalings that has been proposed to hold in the fully universal Efimov scenario [53,81], we apply our combined model to the data of Ref. [53]. In that work, the N-boson system was assumed to interact through a combination of two- and three-body potentials. The resulting transition temperature T_{tr} is shown by squares in Fig. 8. The two cases display different large-N behavior: The transition temperature increases roughly linearly with N for the Gaussian two-body model interaction but increases much slower for the system with two- and three-body interactions. We note that the finite-temperature behavior of the trapped $N = 100$ Bose system was investigated by Piatecki and Krauth using the PIMC approach [82]. In the regime where $|E_{trimer}|$ is much larger than E_{ho}, Ref. [82] finds, in agreement with
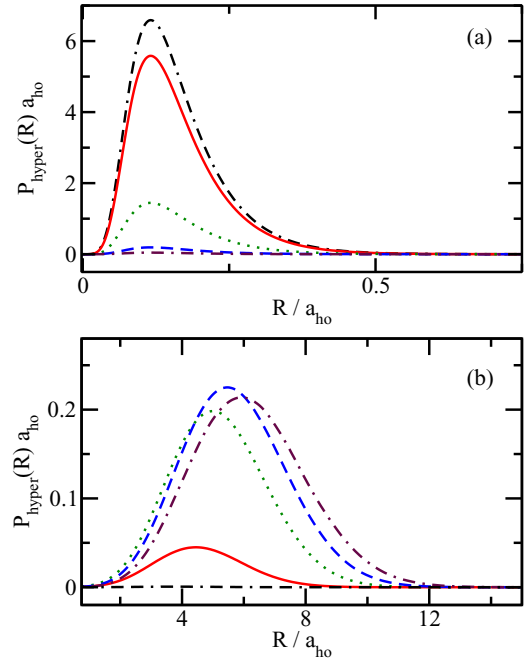

FIG. 9. (Color online) Hyperradial density $P_{hyper}(R)$ for three identical bosons at unitarity interacting through V_G with $r_0 = 0.06a_{ho}$ for various temperatures T. Dash-dash-dotted, solid, dotted, dashed, and dash-dotted lines are for $k_B T/E_{ho} = 3,4,5,6$, and 7, respectively. Panel (a) shows the small-R region while panel (b) shows the large-R region. Note that panels (a) and (b) have different scales for the x and the y axes.

our work, a transition from a droplet state to a gaslike state. Reference [82] refers to the phase that is governed by the droplet state as Efimov liquid phase. We emphasize that our calculations neglect decay to nonuniversal states. Such states would need to be accounted for if one wanted to analyze the stability of the droplet phase.

We now discuss the system characteristics below and above T_{tr} in more detail. As already mentioned in Sec. II B, the hyperradial distribution functions $P_{hyper}(R)$ for the three-boson system interacting through V_G with ranges $r_0 = 0.06a_{ho}$ and $0.1a_{ho}$ at low temperature (see Fig. 2 for $k_B T = 0.4E_{ho}$) are essentially identical to the free-space three-boson systems with the same r_0 at zero temperature. Figure 9 shows the temperature dependence of $P_{hyper}(R)$ for $N = 3$ and $r_0 = 0.06a_{ho}$. The dash-dash-dotted line shows the hyperradial distribution function for $k_B T = 3E_{ho}$, i.e., for a temperature below T_{tr}. For this temperature, $P_{hyper}(R)$ exhibits a maximum at $R \approx 0.15a_{ho}$ and falls off monotonically at larger R. For slightly larger T, i.e., $k_B T = 4E_{ho}$ (solid line), the maximum at $R \approx 0.15a_{ho}$ is smaller and a second peak at $R \approx 4$–$5a_{ho}$ appears. At yet higher T (above the transition temperature), the amplitude of the large-R peak is more pronounced and the hyperradial distribution function resembles that of a gaseous system. The temperature dependence of the hyperradial distribution function for the $N = 3$ system supports our interpretation introduced above, namely, the notion that the system undergoes a transition from an Efimov trimer to a gas state as the temperature changes from below to above T_{tr}. The hyperradial distribution
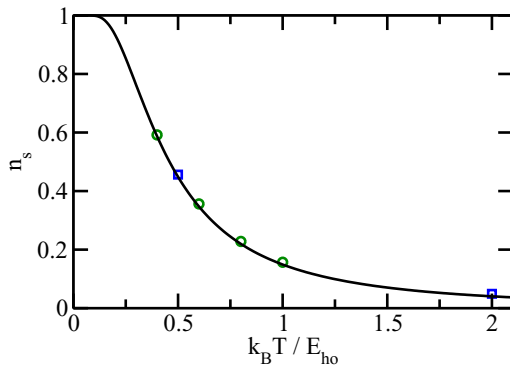
FIG. 10. (Color online) Superfluid fraction n_s as a function of the temperature T for N identical bosons at unitarity. The circles and squares show the PIMC results for the Gaussian potential V_G with $r_0 = 0.1a_{\mathrm{ho}}$ for $N = 3$ and 4, respectively. The error bars are smaller than the symbol size. For comparison, the solid line shows the result obtained using a single-particle model (see text for discussion).

functions for larger systems show analogous behavior, i.e., they support the notion that the system undergoes a transition from an N-body droplet state to a gas state with increasing temperature.

To further characterize the properties of the N-boson system, symbols in Fig. 10 show the superfluid fraction n_s as a function of the temperature for $N = 3$ and 4 obtained using the PIMC approach (here, $r_0 = 0.1a_{\mathrm{ho}}$ and $1/a_s = 0$). The superfluid fractions for these two system sizes seem to fall on one curve. The solid line, which is obtained analytically (see the following discussion for the model that produces the solid line), provides a good description of the numerical data. Figure 10 suggests that the superfluid fraction approaches one in the zero-temperature limit and is smaller than 0.05 for $k_B T \gtrsim 2E_{\mathrm{ho}}$. From Figs. 6 and 7 and the surrounding discussion, we know that the temperature regime $k_B T \lesssim 2E_{\mathrm{ho}}$ is, for the parameters considered, well described by the partition function Z_{droplet}, i.e., the system behavior is dominated by the lowest N-droplet energy eigenstate and its center-of-mass excitations. In particular, this means that the droplet itself can be considered as "frozen." Correspondingly, we expect that the behavior of the superfluid fraction displayed in Fig. 10 is approximately described by that of a single harmonically trapped particle of mass Nm_{a} (see the solid line in Fig. 10). We observe that the PIMC points lie slightly above the solid line. This could be due to the fact that the classical moment of inertia calculated using the single-particle framework is slightly smaller than the classical moment of inertia calculated using the full Hamiltonian.

We now relate the falloff of the superfluid fraction to the transition temperature. As discussed above, the falloff of n_s is governed by center-of-mass excitations, i.e., the relevant temperature scale is set by the harmonic oscillator frequency. To make some estimates, we say that the superfluid fraction, defined through the moment of inertia, is "undetectably small" for $k_B T$ around $2E_{\mathrm{ho}}$, independent of the number of particles and interaction model. This estimate assumes that the absolute value of the eigenenergy of the lowest droplet state is large enough for Z_{droplet} to provide a reasonably accurate description

of the low-temperature dynamics. For the three- and four-body systems, this implies that $|E_{\mathrm{droplet}}|$ has to be larger than a few times E_{ho}. For cold atom systems, the three-body parameter is found to be approximately universal [51,83,84], i.e., $a_- \approx -9.7R_{\mathrm{vdW}}$, where R_{vdW} denotes the van der Waals length and a_- the scattering length at which the Efimov trimer merges with the three-atom continuum. Using this approximate universality together with the known relation between a_- and κ_* [18], we estimate that E_{trimer} is roughly equal to $-0.024E_{\mathrm{vdW}}$ at unitarity. Here, E_{vdW} is defined as $E_{\mathrm{vdW}} = \hbar^2/(m_{\mathrm{a}}R_{\mathrm{vdW}}^2)$. For Cs in a spherically symmetric harmonic trap with a frequency $\nu \approx 2$ kHz (a value that can be reached easily), the Efimov trimer would have an energy of about $-33E_{\mathrm{ho}}$ (the system is approximately described by the circles in Fig. 6). For these experimental conditions, the superfluid fraction is vanishingly small for $T \gtrsim T_{\mathrm{tr}}$.

A key ingredient of the above analysis is that the falloff of the superfluid fraction is due to the center-of-mass excitations. This suggests an alternative viewpoint that defines the superfluid fraction with respect to the relative degrees of freedom only. If we replace the z component $\hat{L}_{\mathrm{tot},z}$ of the total orbital angular momentum operator in Eq. (14) by the z component of the relative orbital angular momentum operator and modify the definition of the classical moment of inertia accordingly, then we find that the falloff of the superfluid fraction is correlated with the transition temperature. The spirit of the latter approach underlies the arguments of Ref. [82], which considers a Bose gas with $N = 100$ and refers to the phase governed by the N-droplet state as superfluid phase. We emphasize, however, that Ref. [82] did not perform any quantitative calculations of the superfluid fraction or superfluid properties of the system. Instead, Ref. [82] put forward qualitative arguments based on the exchange paths.

We reiterate that the combined model breaks down when $|E_{\mathrm{droplet}}|$ is not much larger than E_{ho}, i.e., when the size of the trimer approaches the harmonic oscillator length. In this case, the lowest Efimov trimer does not define a separate energy scale and the phase-transition-like feature discussed in this work disappears. Qualitatively, we expect that the Bose gas with $N = 3, 4, \ldots$ changes from having a significant superfluid fraction to a small superfluid fraction as the temperature increases from zero to a few times E_{ho}. The $N = 100$ case has been considered in Ref. [82].

B. Single-component gas with a single impurity

This section considers a single-component gas consisting of $N - 1$ particles with an impurity. We assume that the impurity interacts with the $N - 1$ "background" atoms through the Gaussian potential V_G with diverging s-wave scattering length a_s. The background atoms do not interact with each other. Our goal is to investigate the temperature dependence of the system properties as the statistics of the $N - 1$ background atoms changes from Bose to Boltzmann to Fermi statistics. As before, we consider equal mass systems. Efimov trimers do not exist for two identical fermions and a third distinguishable particle (in our case, the impurity) [18,85]. For two identical bosons and a third particle or two Boltzmann particles (i.e., two distinguishable particles) and a third particle, however, Efimov trimers can exist [86]. An interesting question is thus

how the finite-temperature properties of the $(N-1,1)$ system with $N \geqslant 3$ depend on the statistics.

From the discussion in the previous subsection it is clear that the properties of the trimer at low temperature determine the characteristics of larger Bose systems provided $|E_{trimer}|$ is much larger than E_{ho}. Throughout this section, we consider the situation where the lowest-energy eigenstate of the $(2,1)$ system with Bose statistics has an energy comparable to E_{ho}, i.e., $|E_{trimer}| \approx E_{ho}$ [note, the lowest-energy eigenstate of the $(2,1)$ system with Boltzmann statistics has the same energy]. For the same model interactions, the lowest-energy eigenstate of the $(2,1)$ system with Fermi statistics also has an energy comparable to E_{ho}; the energy for the system with Fermi statistics is, however, larger than that for the system with Bose statistics. We will show that the low-temperature properties of the $(N-1,1)$ systems display, as might be expected naively, statistics-dependent characteristics for temperatures around or below E_{ho}. Concretely, we focus on systems with interspecies Gaussian interactions with $r_0 = 0.06 a_{ho}$ and $1/a_s = 0$. The relative ground-state energy of the harmonically trapped $(2,1)$ system with Bose statistics is $0.508 E_{ho}$ [or $141\hbar^2/(mr_0^2)$]. For comparison, the relative ground-state energy of the corresponding free-space system is $-18.1\hbar^2/(mr_0^2)$, indicating that the trap modifies the lowest-energy eigenstate of the free-space system with Efimov characteristics. The relative ground-state energy of the harmonically trapped $(2,1)$ system with Fermi statistics is $2.785 E_{ho}$. The corresponding free-space system is not bound [6].

Figure 11 shows the scaled pair distribution functions $r_{j4}^2 P_{pair}(r_{j4})$, $j < 4$, for the $(3,1)$ system with $r_0/a_{ho} = 0.06$ and $1/a_s = 0$ for different statistics and temperatures. The dotted, dashed, and solid lines are for Bose, Fermi, and Boltzmann statistics, respectively. Figures 11(a)–11(d) are for $k_B T/E_{ho} = 0.6$, 1.2, 2, and 3, respectively. At high temperature [see Fig. 11(d)], the pair distribution functions are to a very good approximation independent of the particle statistics. As the temperature decreases [see Fig. 11(c)], the particle statistics has a visible effect on the pair distribution functions. In the PIMC language, the temperature in Fig. 11(c) is such that the "permuted paths" contribute only a small fraction to the partition function. This implies that the particle statistics can be treated perturbatively, i.e., the partition functions $Z_{Bose}(\beta)$ and $Z_{Fermi}(\beta)$ of the systems with Bose and Fermi statistics can be written approximately as $[Z_{Boltz}(\beta) \pm \Delta Z(\beta)]/3!$, where $Z_{Boltz}(\beta)$ denotes the partition function of the system with Boltzmann statistics and $\Delta Z(\beta)$ a small correction. The factor of $1/3!$ arises due to the presence of the three identical particles (bosons or fermions). Correspondingly, the sum of the energies of the systems with Bose and Fermi statistics equal, to a good approximation, twice the energy of the system with Boltzmann statistics. Indeed, for the temperature considered in Fig. 11(c), we find $E/E_{ho} = 23.86(2)$, 23.33(2), and 22.76(1) for Fermi, Boltzmann, and Bose statistics, respectively. The energy differences are 0.53(4) and 0.57(3), in agreement with the expectation based on the perturbative argument.

For yet lower temperatures, the particle statistics becomes nonperturbative. In Fig. 11(b), e.g., the pair distribution functions for the three different statistics differ notably. In Fig. 11(a), the pair distribution functions for the systems with Boltzmann and Bose statistics are nearly indistinguishable and
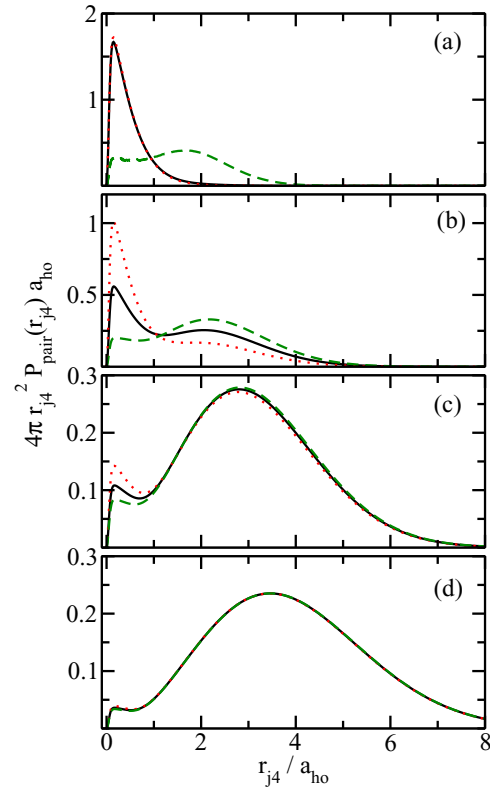

FIG. 11. (Color online) Scaled pair distribution functions $r_{j4}^2 P_{pair}(r_{j4})$ ($j < 4$) for the $(3,1)$ system with interspecies interaction V_G with $r_0 = 0.06 a_{ho}$ and diverging interspecies scattering length a_s at temperature (a) $k_B T/E_{ho} = 0.6$, (b) $k_B T/E_{ho} = 1.2$, (c) $k_B T/E_{ho} = 2$, and (d) $k_B T/E_{ho} = 3$. Dashed, solid, and dotted lines are for systems with Fermi, Boltzmann, and Bose statistics, respectively. The error bars are comparable to or smaller than the linewidths. In panel (a), the solid and dotted lines are hardly distinguishable. In panel (d), all three lines nearly coincide.

notably different from the pair distribution function for the system with Fermi statistics. This can be explained as follows. The systems with Bose and Boltzmann statistics have the same ground-state energy while the system with Fermi statistics has a notably larger ground-state energy. Due to the absence of bound trimer states for the system with Fermi statistics for vanishing confinement (i.e., for $w = 0$), the pair distribution function is fully determined by the trap length and the temperature [4–6]. For the systems with Bose and Boltzmann statistics, the pair distribution function takes on large values at small r, reflecting the fact that these systems form a dropletlike state for vanishing confinement. An important consequence is that the two-body contacts for the systems with Bose and Boltzmann statistics are, in the low-temperature regime, much larger than the two-body contact for the system with Fermi statistics.

Symbols in Fig. 12 show the superfluid fraction n_s as a function of the temperature for the $(3,1)$ system with interspecies potential V_G with $r_0 = 0.06 a_{ho}$ and infinitely large s-wave scattering length. Circles, crosses, and squares are for Bose, Boltzmann, and Fermi statistics, respectively. As the temperature decreases, the superfluid fraction increases for the systems with Boltzmann and Bose statistics and reaches
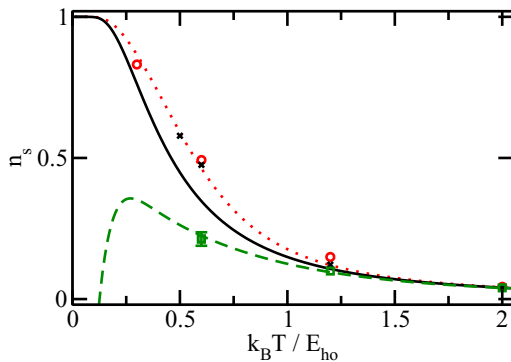
FIG. 12. (Color online) Superfluid fraction n_s as a function of the temperature T for the (3,1) system with interspecies potential V_G with $r_0 = 0.06a_{ho}$ and $1/a_s = 0$. The circles, crosses, and squares are obtained from the PIMC simulations with Bose, Boltzmann, and Fermi statistics, respectively. The error bars are only shown when they are larger than the symbol size. For comparison, dotted, solid, and dashed lines show the superfluid fraction for the noninteracting (3,1) systems with Bose, Boltzmann, and Fermi statistics, respectively.

1 at zero temperature. The superfluid fraction of the (3,1) system with Fermi statistics lies below that for the (3,1) system with Bose and Boltzmann statics at high temperature. Our calculations go down to $k_B T = 0.6 E_{ho}$. Based on our earlier work [65], we expect that the superfluid fraction for the system with Fermi statistics will take on negative values as the temperature approaches zero. At high temperature, the perturbative analysis, introduced earlier for the energy, can be applied to the superfluid fraction. The "permuted paths" contribute perturbatively to the quantum moment of inertia and the classical moment of inertia. The combination of the two gives rise to a correction of the superfluid fraction calculated from the "unpermuted paths," i.e., a correction to the superfluid fraction for the (3,1) systems with Boltzmann statistics due to the exchanges of identical particles. At $k_B T = 2 E_{ho}$, we find $n_s = 0.039\,76(5)$, $0.041\,32(1)$, and $0.042\,94(3)$ for the (3,1) systems with Fermi, Boltzmann, and Bose statistics, respectively. The differences are $0.001\,56(6)$ and $0.001\,62(4)$, in agreement with the expectation based on the perturbative argument. For comparison, dotted, solid, and dashed lines show the superfluid fraction for the noninteracting (3,1) systems with Bose, Boltzmann, and Fermi statistics, respectively. For the system with Bose statistics, the unitary interactions change the superfluid fraction only slightly. For the system with Boltzmann statistics, the interactions have a notably larger effect on the superfluid fraction. The nontrivial shift comes from the interplay between the temperature and the interactions.

Finally, we comment that the single-particle model, where the droplet is described as a single particle of mass $N m_a$, is not applicable. The superfluid fraction for this model coincides with the solid line in Fig. 12. If $|E_{trimer}|$ was much larger than E_{ho}, we would expect that the superfluid fraction for the systems with Bose and Boltzmann statistics would follow the solid line. The fact that the symbols deviate from the solid line indicates that the single-particle model is not applicable. Interestingly though, the superfluid fraction seems to only change weakly as E_{trimer}/E_{ho} changes, suggesting that n_s is

not a sensitive probe of the phase-transition-like feature or absence thereof.

V. CONCLUSIONS

This paper considered the finite-temperature properties of small s-wave interacting systems under spherically symmetric harmonic confinement. For two particles in the harmonic trap, we compared the condensate and superfluid fractions as a function of the temperature. The role of the particle statistics on these quantities was discussed. For two Boltzmann particles, the condensate fraction exhibits a strong dependence on the interaction strength, while the superfluid fraction is only weakly dependent on the interaction strength. Changing from Boltzmann to Bose statistics changes the observables by a relatively small amount, while changing from Boltzmann to Fermi statistics introduces significant quantitative changes.

We further considered N bosons with finite-range two-body Gaussian interactions at unitarity in the regime where the absolute value of the N-boson droplet energy $|E_{droplet}|$ is much larger than the harmonic oscillator energy. We observed a sharp transition as the temperature increases from a liquid dropletlike state to a gaslike state. The energy, heat capacity, hyperradial distribution function, and superfluid fraction were monitored as a function of the temperature. A simple model that semiquantitatively captures the entire temperature regime was proposed. The model was not only applied to systems with Gaussian interactions, but also to systems with two- and three-body interactions. No evidence for "intermediate phases" such as a gas consisting of trimers or tetramers was found. Finally, we considered the (3,1) system with infinitely large interspecies scattering length. We compared the pair distribution function for systems with Bose, Boltzmann, and Fermi statistics. We established that the statistics can be treated perturbatively at high temperature.

In the future, it will be interesting to extend the few-body studies presented here to a larger number of particles. For bosons, this should be fairly straightforward. For fermions, however, the sign problem will place constraints on the temperature regime that can be covered. Large weakly interacting trapped N-boson systems at finite temperature have been studied using classical field theory and other approaches [87,88]. These approaches assume that the system is in a gaslike state and capture the shift of the transition temperature from a thermal gas to a Bose-Einstein condensate with the number of particles. These techniques are, however, not applicable when the s-wave scattering length becomes infinitely large. In this regime, beyond mean-field approaches are needed. Earlier work based on the ϵ or $1/N$ expansion [89,90], renormalized interactions [91], and the diffusion Monte Carlo approach [92] treated unitary interactions but were restricted to zero temperature. The PIMC approach employed here and in Ref. [82] provides, in our view, a powerful means to study the finite-temperature behavior of the strongly correlated N-boson system over a wide range of system sizes.

An important question is if the N-boson droplet state discussed here can be probed experimentally. Our calculations excluded nonuniversal energetically lower-lying states, which could lead to atom losses. Moreover, we assumed that the system is in thermal equilibrium. In practice, experimental

investigations will have to work in a parameter regime where the equilibration time is faster than the atom loss time. It remains an open question if quench experiments such as those recently conducted at JILA [93] could, if applied to small systems, probe the phase-transition-like feature discussed in this work. A possible scheme would be to start with a weakly interacting system with known but variable temperature, to jump the magnetic field to unitarity, and last to probe the system after a variable hold time.

Our calculations for few-fermion systems showed that a temperature of less than E_{ho}/k_B leads to notable changes in the structural properties. This suggests that the analysis of few-fermion experiments has to account for finite-temperature effects. A similar conclusion was reached in Refs. [94,95], which

considered (motivated by the Heidelberg experiments [96–98]) the temperature dependence of one-dimensional few-fermion systems.

[1] F. Dalfovo, S. Giorgini, L. P. Pitaevskii, and S. Stringari, Rev. Mod. Phys. **71**, 463 (1999).

[2] C. Pethick and H. Smith, *Bose-Einstein Condensation in Dilute Gases* (Cambridge University Press, Cambridge, UK, 2002).

[3] L. P. Pitaevskii and S. Stringari, *Bose-Einstein Condensation* (Oxford University Press, Oxford, UK, 2003).

[4] I. Bloch, J. Dalibard, and W. Zwerger, Rev. Mod. Phys. **80**, 885 (2008).

[5] S. Giorgini, L. P. Pitaevskii, and S. Stringari, Rev. Mod. Phys. **80**, 1215 (2008).

[6] D. Blume, Rep. Prog. Phys. **75**, 046401 (2012).

[7] D. Tilley and J. Tilley, *Superfluidity and Superconductivity*, Graduate Student Series in Physics (IOP Publishing, Bristol, 1990).

[8] A. J. Leggett, *Quantum Liquids* (Oxford University Press, Oxford, UK, 2006).

[9] M. Greiner, C. A. Regal, and D. S. Jin, Nature (London) **426**, 537 (2003).

[10] M. W. Zwierlein, C. A. Stan, C. H. Schunck, S. M. F. Raupach, S. Gupta, Z. Hadzibabic, and W. Ketterle, Phys. Rev. Lett. **91**, 250401 (2003).

[11] P. Ring and P. Schuck, *The Nuclear Many-Body Problem* (Springer, Berlin, 2004).

[12] R. Pathria, *Statistical Mechanics* (Elsevier, Amsterdam, 1996).

[13] H. B. Callen, *Thermodynamics and an Introduction to Thermostatistics* (Wiley, Hoboken, NJ, 2006).

[14] D. S. Petrov, Phys. Rev. A **67**, 010703(R) (2003).

[15] J. Carlson, S.-Y. Chang, V. R. Pandharipande, and K. E. Schmidt, Phys. Rev. Lett. **91**, 050401 (2003).

[16] G. E. Astrakharchik, J. Boronat, J. Casulleras, and S. Giorgini, Phys. Rev. Lett. **93**, 200404 (2004).

[17] V. Efimov, Phys. Lett. B **33**, 563 (1970).

[18] E. Braaten and H.-W. Hammer, Phys. Rep. **428**, 259 (2006).

[19] K. Huang and C. N. Yang, Phys. Rev. **105**, 767 (1957).

[20] D. M. Ceperley, Rev. Mod. Phys. **67**, 279 (1995).

[21] G. Baym, *Lectures on Quantum Mechanics*, Advanced Book Program (Addison-Wesley, Boston, 1990).

[22] In *Mathematica*, the number of inversions $N_I(\sigma)$ is represented by the function Inversions.

[23] For the two-component system, normalization to the number of particles in each component would be a more natural choice.

[24] O. Penrose and L. Onsager, Phys. Rev. **104**, 576 (1956).

[25] M. Girardeau, J. Math. Phys. **1**, 516 (1960).

[26] K. M. Daily, X. Y. Yin, and D. Blume, Phys. Rev. A **85**, 053614 (2012).

[27] M. A. Cirone, K. Góral, K. Rzążewski, and M. Wilkens, J. Phys. B: At., Mol. Opt. Phys. **34**, 4571 (2001).

[28] A. Cherny, J.-S. Caux, and J. Brand, Front. Phys. **7**, 54 (2012).

[29] I. Carusotto, Physics **3**, 5 (2010).

[30] A. Wairegi, A. Gamboa, A. D. Burbanks, E. A. Lee, and D. Farrelly, Phys. Rev. Lett. **112**, 143401 (2014).

[31] A. J. Leggett, Phys. Rev. Lett. **25**, 1543 (1970).

[32] G. Baym, in *Mathematical Methods in Solid State and Superfluid Theory*, edited by R. Clark and E. Derrick (Oliver and Boyd, Edinburgh, 1969).

[33] A. J. Leggett, Phys. Fenn. **8**, 125 (1973).

[34] E. L. Pollock and D. M. Ceperley, Phys. Rev. B **36**, 8343 (1987).

[35] Y. Kwon, F. Paesani, and K. B. Whaley, Phys. Rev. B **74**, 174522 (2006).

[36] S. Grebenev, J. P. Toennies, and A. F. Vilesov, Science **279**, 2083 (1998).

[37] S. Grebenev, B. Sartakov, J. P. Toennies, and A. F. Vilesov, Science **289**, 1532 (2000).

[38] J. Tang, Y. Xu, A. R. W. McKellar, and W. Jäger, Science **297**, 2030 (2002).

[39] Y. Kwon and K. B. Whaley, Phys. Rev. Lett. **89**, 273401 (2002).

[40] F. Paesani, Y. Kwon, and K. B. Whaley, Phys. Rev. Lett. **94**, 153401 (2005).

[41] F. Mezzacapo and M. Boninsegni, Phys. Rev. A **75**, 033201 (2007).

[42] F. Mezzacapo and M. Boninsegni, Phys. Rev. Lett. **100**, 145301 (2008).

[43] P. Sindzingre, M. L. Klein, and D. M. Ceperley, Phys. Rev. Lett. **63**, 1601 (1989).

[44] E. W. Draeger and D. M. Ceperley, Phys. Rev. Lett. **90**, 065301 (2003).

[45] F. Werner and Y. Castin, Phys. Rev. Lett. **97**, 150401 (2006).

[46] F. Werner and Y. Castin, Phys. Rev. A **74**, 053604 (2006).

[47] L. H. Thomas, Phys. Rev. **47**, 903 (1935).

[48] S. Jonsell, H. Heiselberg, and C. J. Pethick, Phys. Rev. Lett. **89**, 250401 (2002).

[49] J. Portegies and S. Kokkelmans, Few-Body Syst. **51**, 219 (2011).

[50] Note that the range of the three-body phase θ_b in Fig. 9 of Ref. [6] is incorrect: The unique θ_b values span a range of π instead of 2π.

[51] P. Naidon, S. Endo, and M. Ueda, Phys. Rev. Lett. **112**, 105301 (2014).

[52] A. Kievsky and M. Gattobigio, Phys. Rev. A **87**, 052719 (2013).

[53] J. von Stecher, J. Phys. B: At., Mol. Opt. Phys. **43**, 101002 (2010).

[54] S. A. Chin, Phys. Lett. A **226**, 344 (1997).

[55] S. Jang, S. Jang, and G. A. Voth, J. Chem. Phys. **115**, 7832 (2001).

[56] W. Krauth, *Statistical Mechanics: Algorithms and Computations*, Oxford Master Series in Physics (Oxford University Press, Oxford, UK, 2006).

[57] D. M. Ceperley and E. L. Pollock, Phys. Rev. Lett. **56**, 351 (1986).

[58] E. Y. Loh, J. E. Gubernatis, R. T. Scalettar, S. R. White, D. J. Scalapino, and R. L. Sugar, Phys. Rev. B **41**, 9301 (1990).

[59] For identical fermions, our S is equal to the quantity $\langle S \rangle_{\bar{P}}$ of Ref. [58].

[60] D. M. Ceperley, in *Monte Carlo and Molecular Dynamics of Condensed Matter Systems*, edited by K. Binder and G. Ciccotti (Editrice Compositori, Bologna, Italy, 1996).

[61] D. Ceperley and B. Alder, Science **231**, 555 (1986).

[62] D. Ceperley, J. Stat. Phys. **63**, 1237 (1991).

[63] T. Busch, B.-G. Englert, K. Rzążewski, and M. Wilkens, Found. Phys. **28**, 549 (1998).

[64] X. Waintal, G. Fleury, K. Kazymyrenko, M. Houzet, P. Schmitteckert, and D. Weinmann, Phys. Rev. Lett. **101**, 106804 (2008).

[65] Y. Yan and D. Blume, Phys. Rev. Lett. **112**, 235301 (2014).

[66] Y. Kwon, P. Huang, M. V. Patel, D. Blume, and K. B. Whaley, J. Chem. Phys. **113**, 6469 (2000).

[67] E. Lee, D. Farrelly, and K. B. Whaley, Phys. Rev. Lett. **83**, 3812 (1999).

[68] W. K. Wootters, Phys. Rev. Lett. **80**, 2245 (1998).

[69] A. Peres, Phys. Rev. Lett. **77**, 1413 (1996).

[70] B. Sun, D. L. Zhou, and L. You, Phys. Rev. A **73**, 012336 (2006).

[71] I. Talmi, Helv. Phys. Acta **25**, 185 (1952).

[72] M. Moshinsky, Nucl. Phys. **13**, 104 (1959).

[73] A. Migdal, Nucl. Phys. **13**, 655 (1959).

[74] Y. Alhassid, G. F. Bertsch, L. Fang, and S. Liu, Phys. Rev. C **72**, 064326 (2005).

[75] M. H. W. Chan, K. I. Blum, S. Q. Murphy, G. K. S. Wong, and J. D. Reppy, Phys. Rev. Lett. **61**, 1950 (1988).

[76] E. Burovski, E. Kozik, A. Kuklov, N. Prokof'ev, and B. Svistunov, Phys. Rev. Lett. **94**, 165301 (2005).

[77] Ş. G. Söyler, B. Capogrosso-Sansone, N. V. Prokof'ev, and B. V. Svistunov, Phys. Rev. A **76**, 043628 (2007).

[78] A. Deltuva, Few-Body Syst. **54**, 569 (2013).

[79] M. Gattobigio and A. Kievsky, arXiv:1309.1927.

[80] D. Rakshit, K. M. Daily, and D. Blume, Phys. Rev. A **85**, 033634 (2012).

[81] Note that Refs. [79, 99] propose that the N-boson droplet energy scales as $N(N-1)$ in the universal regime.

[82] S. Piatecki and W. Krauth, Nat. Commun. **5**, 3503 (2014).

[83] J. Wang, J. P. D'Incao, B. D. Esry, and C. H. Greene, Phys. Rev. Lett. **108**, 263001 (2012).

[84] P. Naidon, S. Endo, and M. Ueda, arXiv:1208.3912.

[85] V. Efimov, ZhETF Pis. Red. **16**, 50 (1972) [JETP Lett. **16**, 34 (1972)].

[86] V. Efimov, Nucl. Phys. A **210**, 157 (1973).

[87] M. Brewczyk, M. Gajda, and K. Rzążewski, J. Phys. B: At., Mol. Opt. Phys. **40**, R1 (2007).

[88] N. P. Proukakis and B. Jackson, J. Phys. B: At., Mol. Opt. Phys. **41**, 203002 (2008).

[89] S.-J. Jiang, W.-M. Liu, G. W. Semenoff, and F. Zhou, Phys. Rev. A **89**, 033614 (2014).

[90] P. Nikolić and S. Sachdev, Phys. Rev. A **75**, 033608 (2007).

[91] J. J. R. M. van Heugten and H. T. C. Stoof, arXiv:1302.1792.

[92] M. Rossi, L. Salasnich, F. Ancilotto, and F. Toigo, Phys. Rev. A **89**, 041602(R) (2014).

[93] P. Makotyn, C. Klauss, D. Goldberger, E. Cornell, and D. Jin, Nat. Phys. **10**, 116 (2014).

[94] T. Sowiński, T. Grass, O. Dutta, and M. Lewenstein, Phys. Rev. A **88**, 033607 (2013).

[95] T. Sowiński, M. Gajda, and K. Rzążewski, arXiv:1406.0400.

[96] F. Serwane, G. Zürn, T. Lompe, T. B. Ottenstein, A. N. Wenz, and S. Jochim, Science **332**, 336 (2011).

[97] G. Zürn, F. Serwane, T. Lompe, A. N. Wenz, M. G. Ries, J. E. Bohn, and S. Jochim, Phys. Rev. Lett. **108**, 075303 (2012).

[98] A. N. Wenz, G. Zürn, S. Murmann, I. Brouzos, T. Lompe, and S. Jochim, Science **342**, 457 (2013).

[99] A. N. Nicholson, Phys. Rev. Lett. **109**, 073003 (2012).